

Formation of Zinc Inverted Opals on Indium Tin Oxide and Silicon Substrates by Electrochemical Deposition

Beatriz H. Juárez and Cefe López*

Instituto de Ciencia de Materiales de Madrid C/ Sor Juana Inés de la Cruz 3, 28049 Madrid, Spain

Concepción Alonso

Departamento de Química Física Aplicada, Universidad Autónoma de Madrid, Cantoblanco, 28049 Madrid, Spain

Received: June 11, 2004; In Final Form: August 19, 2004

Zinc inverted opals have been fabricated by means of electrochemical deposition templated on polystyrene artificial opals grown on indium tin oxide (ITO) and n-doped silicon substrates. Several differences in the infiltration were observed between samples infilled by linear cyclic voltammetry and square wave pulsating potential approaches, leading to the fabrication of metallic photonic crystals with different topologies on semiconducting substrates. The samples have been characterized by scanning electronic microscopy (SEM), energy dispersive X-ray analysis (EDX), and X-ray powder diffraction. This is the first time that Zn inverse opals have been fabricated and this work proves the possibility of growing macroporous structures by electrochemical methods on different semiconductor substrates.

I. Introduction

Macroporous materials have gathered great attention in the past decades due to the promising future in many areas such as catalysis,¹ chemical sensors,² and photonic crystals.³ In the latter case, large photonic band gaps are predicted for periodic metallic structures opening up new alternatives in the development of potential photonic applications.^{4–7} Measuring and interpreting the optical response of metallic photonic crystals has become a challenging task.^{8–11} Due to the large refractive index, complete photonic band gaps (CPBG) can be opened in regions where the metal absorption is negligible. In thin periodic metallic structures, new interesting phenomena can be expected from the interaction of light with plasmon resonances.¹²

Owing to several reasons—they are widely used, profusely investigated, cheap, and easily fabricated—artificial opals are excellent systems to study the physics involved in the optical response of metallic photonic crystals. Electrodeposition deserves special attention due to its low cost, low-temperature working conditions, and precise control over the thickness and composition of the electrogenerated material. It is a suitable method to grow metals, semiconductors, alloys, and a large number of different compounds. Braun and Wiltzius¹³ used this approach to infill II–VI compounds in silica opals. Bartlett et al.¹⁴ have reported several macroporous structures fabricated by electrochemical methods. Many other authors have used the electrochemical approaches to build up III–V compounds,¹⁵ metallic structures,¹⁶ alloys,¹⁷ semiconductor composites,¹⁸ and conducting polymers¹⁹ based on artificial opals. Electroless baths²⁰ have been employed as well to fill the macroporous bare structures with metals. Other approaches such as photolithography and chemical vapor deposition (CVD) methods were combined to grow one unit cell thick wood-pile arrangements of tungsten.²¹ The metal here reported is of interest not only on

its own but also for the extraordinary optical properties of its oxide. Although ZnO has been electrochemically grown in colloidal templates,²² to the best of our knowledge, this is the first time the growth of Zn inverted opals is reported. ZnO and ZnO/Zn structures derived from Zn opals could be tackled by proper and controlled oxidation of Zn opals in order to study luminescent properties in metallic face-centered cubic (fcc) structures. In this work Zn growth in opals on semiconductor substrates, namely, indium tin oxide (ITO) and n-doped silicon substrates is presented. There is little work concerning the electrodeposition of metallic films on silicon substrates,²³ and to the best of our knowledge, none of them about zinc. Two different electrochemical methods with different growth mechanisms open up the possibility of controlling the fabrication of metallic photonic crystals with different topologies on semiconducting substrates. The growth of periodic metallic zinc on transparent substrates (ITO) and silicon surfaces can be of relevant importance in optoelectronics and other technologies.

Cyclic voltammetry and square wave pulse potential methods²⁴ were used to grow and improve the homogeneity and density of zinc deposits on both substrates. At variance with commercial plating baths that contain additives to improve the final appearance of the deposits, no additives were used in this work. The samples were used as working electrode without masking so that the whole area was allowed for growth.

II. Experimental Section

A. Fabrication of Thin Artificial Opals. Anionic polystyrene spheres were synthesized by a nonsurfactant emulsion polymerization method.²⁵ ITO-coated glass ($R = 10 \Omega \cdot \text{cm}^{-1}$) and n-Si(111) surfaces were used as conducting substrates. Si substrates were cleaved from n-wafers highly doped ($R < 20 \Omega \cdot \text{cm}^{-1}$). The native oxide was removed with 3% vol HF solution for 10 min and finally rinsed with double deionized water. ITO and SiO₂-free silicon substrates were hydrophilized

* Corresponding author. E-mail: cefe@icmm.csic.es.

in two different solutions. SiO₂-free n-Si surfaces were immersed in an acid mixture (H₂SO₄/H₂O₂ 3:1) during 10 min. In the case of ITO substrates a mixture of H₂O/NH₃/H₂O₂ (17:3:1) was used to immerse the samples for 20 min.

The backside of the Si samples was properly preserved from the electrolyte by painting with insulator paste.

Polystyrene (PS) artificial opals were grown by means of the convective method²⁶ to obtain highly ordered fcc structures with controlled thickness. As a typical procedure, in this work 0.3% vol colloids were used, obtaining 5–10 layers of opals after 35 h at 45 °C.

The samples at this stage are not mechanically robust enough to withstand immersion in a liquid without being partially destroyed. A sintering process at appropriate temperature can improve the mechanical strength of artificial opals.²⁷ However, this treatment is not appropriate for opals attached to a substrate. An alternative method recently described, based on the synthesis of SiO₂ in vapor phase at room temperature,²⁸ shows important advantages over temperature treatments. It produces a SiO₂ film covering the spheres that acts as a framework and strengthens the structure without provoking cracks as sintering procedures do and is compatible with the presence of the supporting substrate.

By means of numerical calculations,²⁹ precise estimations in filling fractions can be done by comparing experimental reflectance spectra from bare and silica-infiltrated opals with the photonic bands (not shown). A mere 8% of the pore volume (2% of the total opal volume or a layer of SiO₂ around 1% of the sphere radius) revealed enough. Although opals grown on both ITO and n-Si substrates were covered with silica, the latter were immersed in diluted HF before acting as working electrodes to remove the native SiO₂. By doing so, the silica shell previously deposited was also partially dissolved. After this process the samples remained mechanically stable.

B. Infiltration of Metallic Zinc. A three-electrode setup was used for zinc electrodeposition. A platinum plate served as auxiliary electrode. All the potentials are quoted with respect to Ag/AgCl reference electrode. The cell was properly deaerated by 99.999% N₂ during 20 min before each experiment. The zinc solution (100 g/L) was prepared from zinc acetate (Aldrich, 99.95%) and ultrapure water (Millipore, 18.2 MΩ). The pH of the solution is 6.3. The experiments were performed in solutions thermostated at 25 and 30 °C with the help of a thermostatic bath.

Two different methods have been used to infiltrate thin artificial opals with metallic zinc: cyclic voltammetry and square wave pulsating potential electrodeposition.

C. Inversion Procedure (Oxygen Plasma Etching). In this study, polystyrene spheres were removed by means of oxygen plasma etching at room temperature to avoid the remainders left by organic solvents such as toluene, styrene, or tetrahydrofuran (THF) after the polystyrene dissolution. Adequate oxygen plasma etching yields cleaner structures. The removing was done in several cycles at room temperature (RT) conditions to avoid metal oxidation. Ten cycles, 2 min each with an oxygen pressure of P_{O₂} = 400 mTorr revealed enough for removing the polystyrene opal without damaging the metallic network.

D. Characterizations. The morphology of the specimens was observed by scanning electron microscopy (SEM). An energy-dispersive X-ray analyzer (EDX) equipped on the SEM was used to determine the compositions. Powder X-ray diffraction was recorded from blank substrates.

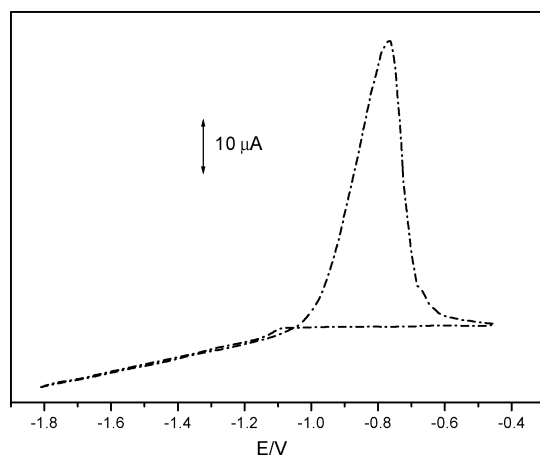


Figure 1. Cyclic voltammetry for n-Si in 100 g/L zinc acetate aqueous solution at pH = 6.3. The scan rate was 10 mV s⁻¹.

III. Results and Discussion

A. Electrochemical Response. Current–potential curves were recorded beforehand in order to choose the optimal working conditions for opals grown on both ITO and n-Si substrates. Regarding the reduction potential, no differences were found between bare substrates and substrates with an opal. Figure 1 shows the voltammogram for a bare n-Si substrate at 30 °C in a 100 g/L zinc acetate aqueous solution. On the initial cathodic scan, zinc deposition starts at -1.05 V, with the current increasing for increasing (more negative) potentials. In these conditions, once a zinc monolayer is formed, bulk zinc deposition takes place. On the other hand, hydrogen evolution reaction on n-Si in background electrolyte (potassium acetate) starts at $E = -1.35$ V. However, this reaction in the presence of zinc is not observed since, once a monolayer has been electrodeposited, the hydrogen development begins taking place on zinc. Hydrogen overpotential on zinc is known to be about 0.7 V ($E_{\text{dH}_2/\text{Zn}} \approx -1.8$ V). This is the reason hydrogen evolution does not interfere with the zinc deposition process.

On the anodic scan, a stripping peak corresponding to the removal of bulk zinc, with an onset at -1.05 V and a current peak centered at -0.77 V, can be seen.

In the case of samples grown on n-Si by cyclic voltammetry, the potential range was -1.05 and -1.35 V at scan rate of 10 mV s⁻¹. Under these conditions, the redissolution of the deposit is prevented. The growth proceeds under kinetic control, avoiding diffusion-limited growth, which is characterized by low-density and high-rugosity deposits.

Voltammograms for ITO substrates were recorded under the same conditions of concentration and temperature (not shown). In the absence of electroactive substance (zinc acetate), the hydrogen evolution reaction starts at $E = -1.2$ V and zinc deposition begins at -1.0 V. The stripping current peak at potential of -0.550 V is observed. However, in this case, the degradation of electrode material occurs just below $E = -1.055$ V. Zn electrodeposition was carried out between -0.850 and -1.055 V, at scan rate of 10 mV s⁻¹. As in the former case, the electrodeposition process does not involve redissolution. The nuclei generated under these conditions grow as the number of scans increases.

Cyclic voltammograms have been recorded as well at 25 °C, showing no differences in the potential range as compared with those at 30 °C.

The square wave pulsating potential method consists of a periodic repetition of overpotential pulses. The pulse cycle is characterized by the pulse potentials, the cathodic deposition

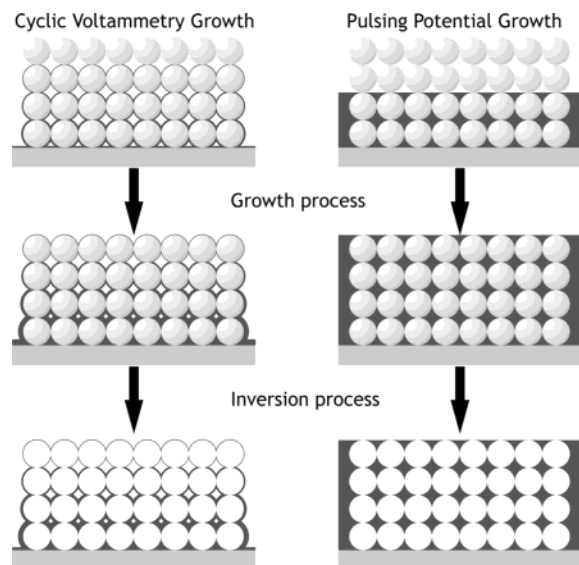


Figure 2. Schematic description of the modes of infiltration of artificial opals: (a) cyclic voltammetry and (b) square wave pulsating potential methods.

time (t_{on}), and the time interval between two pulses (t_{off}), in which the system relaxes.²⁴ According to theory, this method yields smoother uniform surfaces with finer grains as a result of higher instantaneous current densities and is an efficient way to control the particle size distributions. During the on time, the formation of zinc nuclei takes place, and during off time, a recrystallization occurs, obtaining larger grains.

In our case, the pulsed potential waveform applied for zinc deposition on n-Si substrates was $E_{\text{deposition}} = -1.8$ V during $t_{\text{on}} = 1$ ms and $E_{\text{off}} = -1.05$ V during 10 ms. The pause-to-pulse ratio ($p = 10$ ms/1 ms) is 10 and the frequency is 90 Hz. These values are inside a range, optimal to obtain compact deposits, since the depletion in the diffusion layer at the end of the pulse is small and, therefore, there is not influence of mass transport. Besides, the system has time enough (10 ms) to reach a state thermodynamically more stable. For samples on ITO substrates $E_{\text{deposition}} = -1.05$ V and $E_{\text{off}} = -0.85$ V. The deposition time was varied between 2 and 48 h.

B. SEM Characterization of Zinc Inverted Opals. The cyclic voltammetry and pulsing potential electrodeposition approaches are characterized by different ways of infiltration of artificial opals. Feature filling during the Zn deposition under cyclic conditions occurs by growth of an increasingly thicker layer following the spherical geometry of spheres. This approach yields metallic shells around the spheres that become thicker as electrodeposition time evolves. On the other hand, by means of pulsing potential electrodeposition, the electrodeposits nucleate in preferential sites on the substrate around the beads and grow to flood the space between spheres, giving rise to smooth deposits in which opals finally become immersed. Figure 2 clarifies both ways of infiltration. These differences can be related to the previously cited tendencies in the growth of electrodeposits. Since the off time favors the recrystallization, smoother and more uniform surfaces are expected for electrodeposits obtained under pulsating conditions.

On the other hand, cyclic voltammetry yields nuclei that grow as the electrodeposition time increase, giving rise to bigger grains.

Figure 3a shows the first stages of zinc growth by pulsing potential electrodeposition on n-Si inside and outside a single monolayer of opal (after opal removal). Three different zones

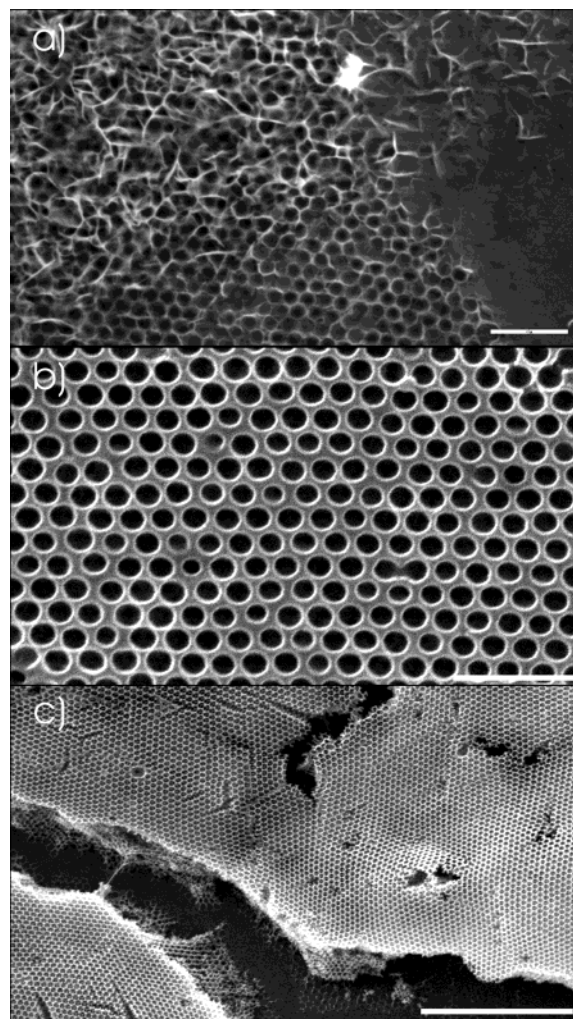


Figure 3. (a) First stages of Zn growth on n-Si under optimized pulsing electrodeposition conditions in the presence/absence of opal template. Scale bar is 2 μm . (b) zinc inverted monolayer on n-Si. Scale bar is 2 μm . (c) Larger area. Scale bar is 10 μm .

can be appreciated: the upper right zone shows the initial steps of Zn growth on opal-free n-Si surfaces. Here, the deposit comprises large needle crystals stacked and randomly oriented, giving rise to an irregular film. On the lower left zone, these wires' growth has been directed by a monolayer of beads (removed upon etching) acting as a template. In the absence of a second layer of spheres, once the cavities between beads have been filled, further growth proceeds again as Zn spikes oriented at random, covering the spheres as in the upper left zone. Figure 3b shows a SEM image of a templated zinc film grown through a single monolayer of 505 nm diameter polystyrene spheres under pulsing conditions during 2 h. The image shows that the spherical voids obtained after removal of the initial pattern are well-ordered and close-packed. The differences in the pore sizes result from film thickness variations in the flooding level. Ordered regions can extend over several hundred square micrometers as can be seen in Figure 3c.

Although not shown, similar SEM images are obtained for samples grown on ITO surfaces. After removal of the initial template, highly ordered and hexagonal structures are obtained. From these pictures it can be clearly observed that the morphology of the deposits is markedly different in the presence of ordered spheres. High quality and smooth deposits are obtained between close-packed beads. As expected, thickness and density of the electrodeposits increase with the electrodeposition time.

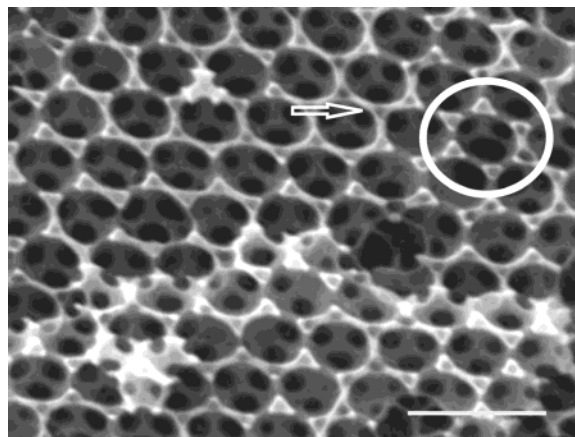


Figure 4. Several stages in the growth of zinc by pulsing electrodeposition. The oblong appearance of some holes is due to the distortion of the metallic lattice under low scanning SEM process. The scale bar is 1 μm .

For short periods of electrodeposition, more open structures are observed with incompletely filled spaces in underneath layers that become filled with time. It is worth noting that pulsing electrodeposition yields very homogeneous surface appearance because higher instantaneous current density provokes an increase in the nucleation rate, leading to the formation of finer-grained deposits. On the other hand, during the off time or relaxing time, the nuclei increase their size due to the diffusion of the adatoms. At variance with Figure 2, which is only a schematic description to clarify the way infiltration proceeds, it is worth mentioning that differences in the stages of growth can be appreciated along the millimeter area of the opal. These deviations allow us to easily understanding the infiltration process. Figure 4 depicts an SEM image of a sample grown by pulsing potential electrodeposition during 8 h on *n*-Si. Several stages of growth can be distinguished.

The picture suggests that, by means of pulsating potential electrodeposition, the Zn nucleation takes place preferentially around the contact points of spheres with the electrode surface, growing forward to the center of the cavities between the beads. In the upper right zone (circled for clarity), six triangles separated by the contact points between the neighbor spheres in a (111) plane can be observed. In this particular point, the thickness of the deposit is in the equator level of the spheres. In every triangle can be seen three nuclei of growth located near the contact points of the spheres corresponding to preferential sites of growth. This geometry leaves an empty dark central spot which is the last space to be filled as the deposit progresses, as can be seen in several points, as the one marked with an arrow.

With increasing film thickness, due to the geometric arrangement of the spheres, it is possible to observe three windows in the second layer, seen as dark circles, in each spherical cavity. These small holes are the internal channels between macropores, resulting from points where the original spheres were in contact in the initial opal.

Relevant differences are observed in opals infilled with zinc by means of cyclic voltammetry. Figure 5 illustrates two stages in the process of Zn growth in opals laying on ITO and *n*-Si substrates under cyclic voltammetry conditions. Figure 5a shows a (111) surface area from an opal infiltrated for 20 h by cyclic voltammetry on an ITO surface (after oxygen plasma inversion). It can be clearly seen that the electrodeposits grow in a conformal way around the beads, replicating the spherical morphology. Thus, in a particular layer, triangular voids between

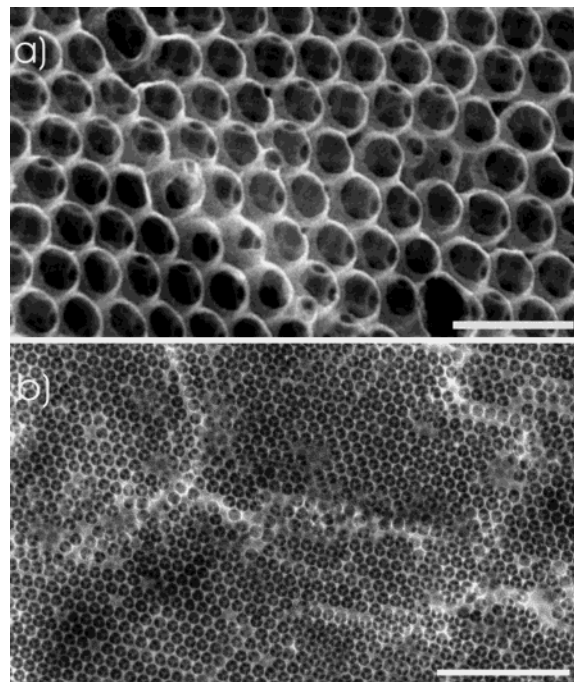


Figure 5. (a) (111) surface in a zinc inverted opal obtained by means of cyclic voltammetry on ITO surface. (b) (111) Zn inverted surface on *n*-Si surface. Scale bars are 1.2 and 5 μm , respectively.

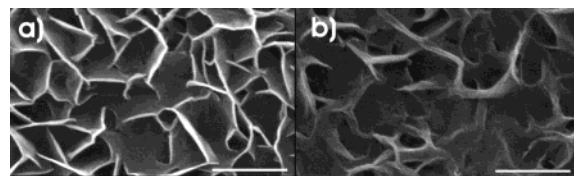


Figure 6. Zinc deposits on *n*-Si at (a) 25 $^{\circ}\text{C}$ and (b) 30 $^{\circ}\text{C}$ under identical experimental conditions. Scale bar is 1 μm .

adjacent spheres are usually empty and bounded by zinc shells. However, further evolution of the electrodeposits with time evidence the complete infilling of pores in underneath layers, which is a sign that the thickness of the deposit is larger in layers closer to the electrode (substrate). Figure 5b depicts a (111) inverted opal surface on *n*-Si. Although the electrodeposits are inhomogeneous in thickness across the whole area of the electrode, which can be due to inhomogeneities in the opal template, large and high-quality areas in the order of hundreds of square micrometers can be obtained. Since the type of growth is shared by opals grown on *n*-Si surfaces and those on ITO, the mode of infiltration is cathode-independent.

C. SEM Characterization of Zinc on Bare Substrates.

Although no significant differences can be appreciated between inverted opals grown at 25 or 30 $^{\circ}\text{C}$, nor in the reduction potentials, marked tendencies can be extracted from the appearance of electrodeposits on blank substrates. Figure 6 shows a nontemplated Zn film on *n*-Si deposited under the same conditions at (a) 25 and (b) 30 $^{\circ}\text{C}$. The increase in temperature favors diffusion of the adatoms, giving rise to smoother deposits.

D. EDX and X-ray Diffraction. EDX analyses optimized for detection of light elements were performed on each sample, confirming the principal presence of zinc in all the structures. However, since commercial ITO films are grown on glass containing oxygen and silicon is naturally oxidized in air, all samples show the presence of oxygen, making it difficult to demonstrate that metallic zinc was not oxidized after the plasma etching. To minimize the detrimental effect derived from the

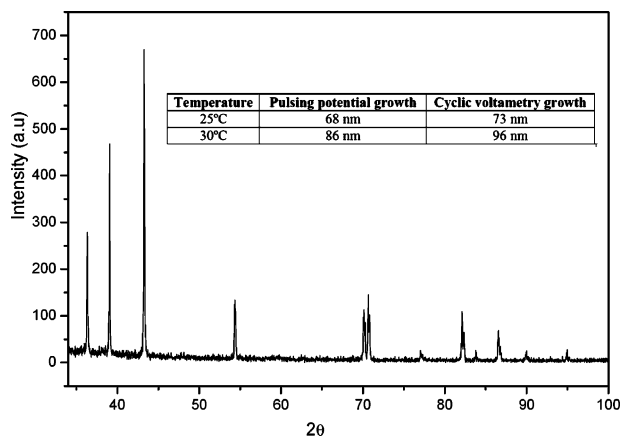


Figure 7. XRD from a free-opal sample obtained at 25 °C by cyclic voltammetry. The inset shows the grain size for samples obtained at 25 and 30 °C under cyclic voltammetry and pulsing potential conditions.

substrates, EDX elemental analysis on bulk zinc obtained under operating conditions identical to those used in the preparation of zinc composites was obtained after 20 and 30 min of oxygen plasma etching. The compositional contents were 92 wt % zinc and 8 wt % oxygen in both cases, confirming that the plasma etching process used does not largely oxidize the electrodeposits (not more, at least, than the natural oxidation in air) and thus, it can be used as an alternative method to remove the organic matrix adequately. The compositional content of zinc in zinc inverted opals varies with the number of layers. In a typical analysis, the zinc content for a monolayer is around 5 wt % and 12–20 wt % for 2–3 layers. The signals coming from the substrates (Si, O, and In) are predominant for a low number of layers.

X-ray diffractograms were collected between 30° and 100° at grazing incidence angle. The crystalline structure of electrodeposits on blank substrates is identified to be hexagonal, in agreement with the known structure for zinc. Figure 7 shows the diffractogram of one such sample obtained by cyclic voltammetry at 25 °C on n-Si.

Similar diffractograms were obtained at 30 °C and the same can be said regarding the square wave pulsating method. The average size of the particles has been derived from the diffractograms by the Scherrer formula. The results are shown in the inset of Figure 7. From these results, it can be concluded that the grain size of the electrodeposits increases as the temperature rises. It can be also appreciated that the square wave pulsating method yields smaller grains under the same conditions.

Again, these results support the theoretical models that predict finer grains for pulse methods as compared to cyclic voltammetry based on the fact that nucleation rates are higher.²⁴

One major advantage of electrodeposition is that the structure does not suffer shrinkage, which implies higher quality inverse opals, obtaining voids consistent with the initial direct structure. When the growth overflows the opal structure, it can be observed that deposits are generated, similar to those occurring in the initial stages (Figure 3a) on blank areas of the electrode, which lead to the formation of zinc platelets. Future tasks will include the study of optimum stripping potentials in order to control the filling fraction of zinc inverted metallic structures.

IV. Conclusions

In summary, zinc inverted opals have been fabricated by electrochemical deposition on semiconductor substrates from polystyrene artificial opals. Linear cyclic voltammetry and

square wave pulsating potential approaches yield different ways of infiltration of these structures. This work demonstrates the possibility of fabricating high-quality metallic structures on semiconductor substrates. Further improvement in the thickness control of the electrodeposits will help us understand the optical behavior of metallic opals.

Acknowledgment. This work is partially financed by the Comunidad Autónoma de Madrid through 07T/0048/2003 and Spanish MCyT through MAT 2003-01237 projects. We thank E. Castillo-Martinez, E. Palacios-Lidón and Dr. D. Golmayo for experimental help.

References and Notes

- (1) Stein, A.; Schroden, R. C. *Curr. Opin. Solid State Mater. Sci.* **2001**, *5*, 553.
- (2) Lee, K.; Asher, S. A. *J. Am. Chem. Soc.* **2000**, *122*, 9534.
- (3) López, C. *Adv. Mater.* **2003**, *15*, 1679.
- (4) (a) Moroz, A. *Phys. Rev. Lett.* **1999**, *83*, 5274. (b) Moroz, A. *Europhys. Lett.* **2000**, *50*, 466.
- (5) Zhang, W. Y.; Lei, X. Y.; Wang, Z. L. *Phys. Rev. Lett.* **2000**, *84*, 2853.
- (6) Li, Z.-Y. *Phys. Rev. B* **2002**, *66*, 214403
- (7) Pralle, M. U.; Moelders, N.; McNeal, M. P.; Puscasu, I.; Greenwald, A. C.; Daly, J. T.; Johnson, E. A.; George, T.; Choi, D. S.; El-Kady, I.; Biswas, R. *Appl. Phys. Lett.* **2002**, *81*, 4685.
- (8) El-Kady, I.; Sigalas, M. M.; Biswas, R.; Ho, K. M.; Soukoulis, C. M. *Phys. Rev. B* **2000**, *62*, 15299.
- (9) Wang, Z.; Chan, C. T.; Zhang, W.; Ming, N.; Sheng, P. *Phys. Rev. B* **2001**, *64*, 113108.
- (10) Li, Z. Y.; El-Kady, I.; Ho, K. M.; Lin, S. Y.; Fleming, J. G. *J. Appl. Phys.* **2003**, *93*, 38.
- (11) von Freymann, G.; John, S.; Schultz-Dobrick, M.; Velkris, E.; Tétreault, N.; Wong, S.; Kitaev, V.; Ozin, G. *Appl. Phys. Lett.* **2004**, *84*, 224.
- (12) Ebbesen, T. W.; Lezec, H. J.; Ghaemi, H. F.; Thio, T.; Wolff, P. A. *Nature* **1998**, *391*, 667.
- (13) Braun, P. V.; Wiltzius, P. *Nature* **1999**, *402*, 603.
- (14) (a) Bartlett, P. N.; Birkin, P. R.; Ghanem, M. A. *Chem. Commun.* **2000**, 1671. (b) Bartlett, P. N.; Baumberg, J. J.; Birkin, P. R.; Ghanem, M. A.; Netti, M. C. *Chem. Mater.* **2002**, *14*, 2199.
- (15) Lee, Y. C.; Kuo, T. J.; Hsu, C. J.; Su, Y. W.; Chen, C. C. *Langmuir* **2002**, *18*, 9942.
- (16) (a) Xu, L.; Zhou, W. L.; Frommen, C.; Baughman, R. H.; Zakhidov, A. A.; Malkinski, L.; Wang, J. Q.; Wiley, J. B. *Chem. Commun.* **2000**, 997. (b) Wijnhoven, J. E. G. J.; Zevenhuizen, S. J. M.; Hendriks, M. A.; Vanmaekelbergh, D.; Kelly, J. J.; Vos, W. L. *Adv. Mater.* **2000**, *12*, 888.
- (17) Luo, Q.; Liu, Z.; Li, L.; Xie, S.; Kong, J.; Zhao, D. *Adv. Mater.* **2001**, *13*, 286.
- (18) van Vugt, L. K.; van Driel, A. F.; Tjerckstra, R. W.; Bechger, L.; Vos, W. L.; Vanmaekelbergh, D.; Kelly, J. J. *Chem. Commun.* **2002**, *18*, 2054.
- (19) Cassagneau, T.; Caruso, F. *Adv. Mater.* **2002**, *14*, 34–38.
- (20) (a) Velev, O. D.; Tessier, P. M.; Lenhoff, A. M.; Kaler, E. W. *Nature* **1999**, *401*, 548. (b) Jiang, P.; Cizeron, J.; Bertone, J. F.; Colvin, V. L. *J. Am. Chem. Soc.* **1999**, *121*, 7957.
- (21) Lin, S. Y.; Fleming, J. G.; Hetherington, D. L.; Smith, B. K.; Biswas, R.; Ho, K. M.; Sigalas, M. M.; Zubrzycki, W.; Kurth, S. R.; Bur, J. *Nature* **1998**, *394*, 251.
- (22) Sumida, T.; Wada, Y.; Kitamura, T.; Yanagida, S. *Chem. Lett.* **2001**, *1*, 138–39.
- (23) (a) Marquez, K.; Ortiz, R.; Schultze, J. W.; Márquez, O. P.; Márquez, J.; Staikov, G. *Electrochim. Acta.* **2003**, *48*, 711. (b) Márquez, K.; Staikov, G.; Schultze, J. W. *Electrochim. Acta.* **2003**, *48*, 875.
- (24) (a) Bard, A. J.; Faulkner, L. R.; Eds. *Electrochemical Methods Fundamentals and Applications*; John Wiley: New York, 1980. (b) Popov, K. I.; Masimovic, M. D. In *Electrochemistry*; Conway, B. E., Bockris, J. O'M., White, R. E., Eds.; Plenum Press: New York, 1989; Vol. XIX, p 193.
- (25) Goodwin, W.; Hearn, J.; Ho, C. C.; Ottewill, R. H. *Colloid Polym. Sci.* **1974**, *252*, 464.
- (26) Jiang, P.; Bertone, J. F.; Hwang, K. S.; Colvin, V. L. *Chem. Mater.* **1999**, *11*, 2132.
- (27) Mayoral, R.; Requena, J.; Moya, J. S.; López, C.; Cintas, A.; Miguez, H.; Meseguer, F.; Vazquez, L.; Holgado, M.; Blanco, A. *Adv. Mater.* **1997**, *9*, 257.
- (28) Míguez, H.; Tétreault, N.; Hatton, B.; Yang, S. M.; Perovic D.; Ozin, G. A. *Chem. Commun.* **2002**, 2736.
- (29) Johnson, S. G.; Joannopoulos, J. D. *Opt. Express.* **2001**, *8*, 173.